Journal of Materials Chemistry C

Accepted Manuscript

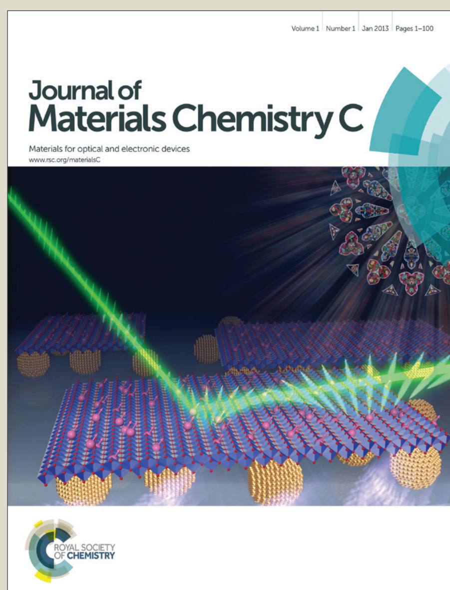

This is an *Accepted Manuscript*, which has been through the Royal Society of Chemistry peer review process and has been accepted for publication.

Accepted Manuscripts are published online shortly after acceptance, before technical editing, formatting and proof reading. Using this free service, authors can make their results available to the community, in citable form, before we publish the edited article. We will replace this *Accepted Manuscript* with the edited and formatted *Advance Article* as soon as it is available.

You can find more information about *Accepted Manuscripts* in the Information for Authors.

Please note that technical editing may introduce minor changes to the text and/or graphics, which may alter content. The journal's standard Terms & Conditions and the Ethical guidelines still apply. In no event shall the Royal Society of Chemistry be held responsible for any errors or omissions in this *Accepted Manuscript* or any consequences arising from the use of any information it contains.

ROYAL SOCIETY OF CHEMISTRY

www.rsc.org/materialsC

Electron transfer induced thermochromism in a VO_2–graphene–Ge heterostructure

Huaijuan Zhou,[a, 1] Jinhua Li,[a, 1] Yunchuan Xin,[a] Xun Cao,[a] Shanhu Bao[a] and Ping Jin[a, b, *]

[a] State Key Laboratory of High Performance Ceramics and Superfine Microstructure, Shanghai Institute of Ceramics, Chinese Academy of Sciences, Shanghai 200050, China

[b] Materials Research Institute for Sustainable Development, National Institute of Advanced Industrial Science and Technology, Nagoya 463-8560, Japan

Corresponding Author:

Prof. Ping Jin

State Key Laboratory of High Performance Ceramics and Superfine Microstructure, Shanghai Institute of Ceramics, Chinese Academy of Sciences, Shanghai 200050, China

E-mail: p-jin@mail.sic.ac.cn; p-jin@aist.go.jp

Tel.: +86 21 6990 6208. Fax: +86 21 6990 6221.

[1] These authors contributed equally to this work.

Journal of Materials Chemistry C Accepted Manuscript

Abstract

As a marvelous thermochromic material, vanadium dioxide (VO_2) holds great promise for applications in smart devices due to semiconductor-metal transition (SMT), an active response to external temperature stimuli and near-infrared irradiation. Here, we demonstrate for the first time that the phase transition temperature of VO_2 film can be effectively manipulated by using graphene as interlayer. High quality graphene monolayer was chemical vapor deposited on Ge underlayer, followed by growing VO_2 film onto graphene to form semimetal-semiconductor contact, namely, a VO_2-graphene-Ge junction. The thermochromic properties of VO_2 film were demonstrated with ~ 20 % infrared reflectance contrast. Furthermore, the transition temperature of VO_2 film was effectively reduced to from 340 K to 330 K. On the basis of the Mott-Hubbard phase transition theory, a plausible mechanism is proposed here for the first time from the perspective of charge transfer to elucidate the experimental phenomenon, which believes that the electron transfer can increase the electron concentration in VO_2 film, destabilize the semiconductor phase of VO_2 film and thus decrease the SMT temperature of thermochromic VO_2 film. In addition to stimulating scientific interest, this study may also contribute to thermochromic VO_2-based applications in sensors, optical and electrical switches, and other nanodevices.

Keywords: Vanadium Dioxide, Thermochromic, Semiconductor-Metal Transition, Graphene, Germanium

Journal of Materials Chemistry C Accepted Manuscript

1. Introduction

Vanadium dioxide (VO_2) is one of the most attractive thermochromic materials, which undergoes a reversible semiconductor-metal transition (SMT) from a high temperature rutile phase ($P4_2/mnm$, R) to a low temperature monoclinic phase ($P2_1/c$, M1) at critical temperature of Tc ~ 340 K.[1, 2] Concomitant with the phase transition is discontinuous jumps in electrical conductivity, optical transmittance, magnetic susceptibility, specific heat, and the Seebeck coefficient.[3, 4] Great efforts have been devoted to the VO_2 thin films due to their extensive applications as well as the enigmatic microscopic mechanism of the phase transition. The Peierls mechanism, which believes the driving force of the SMT in VO_2 is the electron-phonon interaction and the Mott-Hubbard transition which supports the electron-electron interaction are believed to be the two major mechanisms. However, both mechanisms are still under intense debate and many efforts have been made to clarify them.

The microstructure and properties of VO_2 films exhibited strong dependence upon the substrates as well as the buffer layers. The supporting materials such as glass,[5] silicon,[6] sapphire[7] and titanium dioxide[8] are the most frequently used as the substrates for VO_2 films. By varying the substrates, the crystallization behavior (amorphous, polycrystalline or epitaxial film), transition temperature and hysteresis width of the VO_2 films can be regulated. The buffer layer (the interlayer between the substrate and the VO_2 film) also plays a significant role in the behaviors of VO_2 films. Up to present, the buffer layers of SiO_2[9, 10], ZnO[11], SiN_x[12], RuO_2[13], TiO_2[14] and metals (V, W, Fe, Ni, etc.)[15] have been widely investigated. Graphene, recognized as a

Journal of Materials Chemistry C Accepted Manuscript

zero-gap semiconductor (namely, semimetal), is a two-dimensional (2D) hexagonal honeycomb structure and possesses excellent carries mobility (~ 200 000 $cm^2 V^{-1} S^{-1}$) and thermal conductivity (~ 5.0 × 10^3 W $m^{-1} K^{-1}$).[16] Based on its unique properties, one can expect that graphene has the potential to act as a functional buffer layer. However, it is still a mystery how the graphene layer will influence the microstructure and properties of VO_2 films, which needs to be investigated and elucidated.

To date, large-area graphene has been produced on various metal substrates and it is necessary for intended use to transfer the as-grown graphene onto desired substrates.[17] However, these wet-transfer processes may be only feasible for the graphene with small lateral sizes. Also, some additional mechanical stress on graphene is anticipated during the transfer process. To overcome the drawback of undesirable impurities and wrinkle formation during the transfer process, direct synthesis of graphene on required substrate has been explored for practically feasible device applications.[18] As a consequence, it is a scientific action to investigate the microstructure and properties of VO_2 films based on the buffer layer of the graphene without transfer process. Group (IV) semiconductors, including Si and Ge, play a critical role in modern technology, which are widely used in integrated circuits (ICs), chemical sensors, infrared (IR) detectors, and micro-/nanoelectromechanical systems (MEMS/NEMS), etc.. And recently, large-area graphene film was demonstrated to grow directly on Ge layer.[18]

In this work, we attempt to deposit VO_2 thin film on transfer-free Graphene/Ge substrate and investigate the switching behaviors of VO_2 layer. The results show that monolayer graphene

Journal of Materials Chemistry C Accepted Manuscript

can reduce the transition temperature of VO_2 film by ~ 10 K. On the basis of the band theory, we conjecture that this phenomenon is ascribed to the electron injection from graphene to VO_2 film, which leads to a rise of the electron concentration in VO_2. To the best of our knowledge, this work has not been investigated before.

2. Materials and methods

2.1. Fabrication of graphene films

The graphene was prepared by atmospheric pressure chemical vapor deposition (APCVD) technique on 175-μm-thick Ge substrate. Prior to being placed at the center of horizontal quartz tube, the Ge substrates were cut into 2 cm × 2 cm pieces and ultrasonically cleared in the alcohol (Adamas-beta Inc., Shanghai, China) for 10 min. The synthesis was carried out by using a horizontal tube furnace with a quartz processing tube inside (inner diameter of 50 mm). The quartz tube was evacuated to about 10^{-5} mbar and then filled with 200 sccm (sccm denotes standard cubic centimeter per minute at STP) Ar gas (purity, 99.999%) and 50 sccm H_2 gas (purity, 99.999%). After heating to 910 ℃, CH_4 gas (purity, 99.999%) was introduced to grow the graphene for 100 min. Finally, the furnace was cooled to room temperature under the flowing mixture of H_2 and Ar.

2.2. Preparation of VO_2 films

Journal of Materials Chemistry C Accepted Manuscript

The VO_2 films were fabricated through reactive sputtering of 3-inch metal vanadium target with oxygen content of 15 sccm at radio frequency power of 200 W. Before VO_2 films growth process, the deposition chamber was pumped down to ~10^{-4} Pa and pure Ar gas (purity, 99.999%) was introduced at 25 sccm. During the deposition process, the substrates were kept at 450 ℃ for the fine crystallinity of VO_2 thin films and rotated along the vertical axis at a speed of 10 rpm to improve the film homogeneity. After the VO_2 films were deposited, samples were cooled down spontaneously to ambient temperature. The thickness of VO_2 layer was approximately 50 nm.

2.3. Characterization of samples

The graphene layer and VO_2 film were characterized with Raman spectroscopy (Renishaw inVia, UK) under the excitation wavelength of 514 nm with a low output power of 10 mW. Scanning tunnel microscopy (STM; MultiMode 8, BRUKER, USA) was used to obtain the atomic-scale pattern of graphene. The surface morphology was examined by field-emission scanning electron microscopy (FE-SEM; Magellan 400, FEI, USA). The atomic force microscopy (AFM) image was collected using a Nanocute SII scanning probe microscopy operated in tapping mode under ambient conditions. Etched Si nanoprobe tips with spring constant of 40 N/m and resonance frequency of 300 KHz $\pm$ 100 KHz were adopted. The surface chemical compositions and chemical states were determined by X-ray photoelectron spectroscopy (XPS; PHI 5802, Physical Electronics Inc, Eden Prairie, MN). The microstructure and composition of samples were further analyzed on a field-emission transmission electron

Journal of Materials Chemistry C Accepted Manuscript

microscope (TEM; JEM-2100F, JEOL Ltd, Tokyo, Japan) with an accelerating voltage of 200 kV. Graphene film was transferred from Ge substrate onto TEM grids by PMMA-assisted wet-transfer method. Briefly, after etching away the substrate by the mixture of HNO_3 and HF (Adamas-beta Inc., Shanghai, China), the PMMA/graphene layer was transferred to TEM grids, followed by annealing at 50 ℃ for 1.5 h to improve adhesion. The PMMA was then dissolved gradually with acetone (Adamas-beta Inc., Shanghai, China). Finally, the graphene was washed with isopropanol (Adamas-beta Inc., Shanghai, China) for further characterization. The diffuse reflection spectra were recorded by the spectrophotometer (Hitachi Corp., Model UV-4100) equipped with an attachment to control the temperature of the films. The temperature was measured precisely with a temperature sensor in contact with the surface of films, and it was controlled via a temperature controlling unit. Hysteresis loops were measured by collecting the transmittance spectra of samples at a fixed wavelength with a heating rate of ~ 4 ^{o}C /min. Photoluminescence (PL) analysis was conducted using a FluoroMax®-4 fluorescence spectrometer (Horiba Scientific, New Jersey, USA) equipped with a broadband pulsed UV xenon lamp source.

3. Results and discussion

3.1. Graphene characterization

Journal of Materials Chemistry C Accepted Manuscript

The high quality of graphene is essential to assure its practical applications. Herein, Raman microscopy was adopted to characterize the crystalline quality and defect state of the CVD-derived graphene film, as shown in **Figure 1a**. It can be seen that the typical features of graphene, namely, the 2D peak at ~ 2710 cm^{-1} and the G peak at ~ 1580 cm^{-1}, emerge. The absence of D peak (~ 1350 cm^{-1}) indicates that the graphene layer possesses the negligible defect state, in other words, the superior crystalline quality. Cançado et al.[19] have shown that one can successfully determine the crystallite size, L_a (nm), of nanographite by Raman spectroscopy using the general equation $L_a = (2.4\times10^{-10})\lambda^4 (I_D/I_G)^{-1}$, where λ is the laser line wavelength in nanometer units, I_D and I_G are the intensity of the D band and G band, respectively. From the above equation, the crystal domain size of graphene is ~ 4086.2 nm. To further estimate the quality and uniformity of the graphene film on Ge substrate, the intensity ratios of 2D band to G band over a randomly selected area of 25 μm × 25 μm were recorded by Raman mapping method with a spot size of 1 μm and a step size of 1 μm, as shown in **Figure 1b**. The I_{2D}/I_G ratios are quite uniform over the region in the range of 1~2, which, in other words, demonstrates the high quality and superior uniformity of graphene film on Ge at the corresponding scale. **Figure 1c** shows the STM topography of the graphene on Ge with the typical hexagonal lattice at the atomic scale, which originates from the intrinsic feature of graphene. Meanwhile, the high-resolution XPS spectra show that, before graphene deposition, the carbon species on Ge stem from surface contamination, indicated by the C1s peak at 285 eV, typical of the sp^3-bonded carbon (**Figure 1d**). In comparison, for Graphene/Ge, the C1s peak in **Figure 1e** is dominated by

Journal of Materials Chemistry C Accepted Manuscript

the sp^2-bonded carbon at 284.64 eV corresponding to the C1s in graphene.[20] Furthermore, the graphene film was transferred onto the copper grids for TEM analysis to acquire the detailed crystallographic information and layer number. It is observed that the suspended graphene film on the TEM grids is continuous over a large area, as shown in **Figure 1f**. Meanwhile, the inserted SAED (namely, selected area electron diffraction) pattern clearly shows that only one set of hexagonal diffraction pattern exists, demonstrating that the graphene film is single-layer and of high crystalline quality. And, the single-layer characteristic of the graphene film was further been validated by the randomly selected high resolution TEM image of the graphene edge in **Figure 1f**, showing the thickness of ~ 0.34 nm for graphene monolayer.

3.2. VO_2–graphene–Ge characterization

As for the VO_2–graphene–Ge sample, almost all the known Raman modes of monoclinic VO_2 are present, as shown in **Figure 2a**. The Raman band positions are in accordance with prior literature,[21] and no other peaks irrelative to VO_2 phase can be observed, which provides a valid evidence that no other phases have been formed. **Figure 2b** shows the surface topography of the VO_2 film on Graphene/Ge with a thickness of ~ 50 nm measured from the cross-sectional view (**Figure 2c**). From the surface morphology, one can see that structural fluctuation forms on the VO_2 film. In other words, pits and ridges seem on the surface of VO_2 film. To further determine the surface structural feature of VO_2 film, AFM was used to explore the film in tapping mode on a randomly selected region. As shown in **Figure 2d**, interestingly, apparent structural fluctuation

Journal of Materials Chemistry C Accepted Manuscript

of pits and ridges can be seen on the VO_2 film. This type of structural fluctuation is considered to result from the intrinsic wrinkle formation of graphene film,[22, 23] which will be further discussed in **Figure 3**. The RMS (Root-Mean-Square) surface roughness for the VO_2 film on Graphene/Ge is approximately 5 nm.

To determine the valence state of vanadium (V) in the oxide film, XPS examination was performed on the VO_2–graphene–Ge surface. From the high resolution XPS spectrum of V 2p in **Figure 3a**, the valence state of V was confirmed to be +4, and the XPS spectrum indicates two peaks centered at around 516.3 eV and 523.5 eV which correspond to the typical binding energies for V $2p_{3/2}$ and V $2p_{1/2}$ in VO_2, respectively. Meanwhile, the source of carbon species can also be found out from the surface XPS analysis of VO_2–graphene–Ge. As shown in **Figure 3b**, the high resolution C 1s XPS spectrum reveals that the carbon species on the VO_2 film originate from the surface contamination of sp^3-bonded carbon with the C1s peak at 285 eV, which is due to the fact that the thickness of the continuous VO_2 film (~ 50 nm) exceeds the sampling depth of XPS analysis (less than 10 nm). As a consequence, the graphene layer under the VO_2 film cannot be detected by the XPS. In order to define the microstructure of the VO_2–graphene–Ge, we have employed the XRD and HR-TEM characterizations. From the XRD analysis result (not listed here), we found that the VO_2 film on Graphene/Ge mainly consisted of an amorphous phase. **Figure 3c-d** shows the randomly selected cross-sectional TEM image, HR-TEM image and SAED pattern of the VO_2–graphene–Ge. From the corresponding HR-TEM image in **Figure 3d**, the trenchant lattice fringe indicates the excellent crystallinity of the

Journal of Materials Chemistry C Accepted Manuscript

underlying Ge. On the contrary, the VO_2 film grown on graphene support presents an unorderly lattice fringe although some tiny crystallite grains exist, showing the poor crystallization quality further demonstrated by the corresponding SAED pattern. A plausible mechanism is proposed here, that is, the atomic-scale wrinkles of graphene plays a crucial role in the crystallinity of the deposited film.[24-26] At the same time, the VO_2 film grows tightly along the graphene layer and tightly sticks together with the graphene wrinkles. As a result, their interface tightly bonds together without significant microcracks or micropores.

3.3. Thermochromism in VO_2–graphene–Ge heterojunction

The thermochromic properties are clearly exhibited in **Figure 4a**, which shows an obvious reflectance contrast in the near-infrared region. Since the optical properties of Graphene/Ge substrate are insensitive to temperature, the reflectance change is attributed to the thermochromic nature of VO_2 thin film. At the wavelength of 2000 nm, for instance, the reflectance is ~ 32.8 % in the semiconductor phase while it reaches ~ 55.5 % in the metal phase. The plasma frequency (ω_p) for metallic state VO_2 is reported to be 1.0 eV (~ 1240 nm)[27] or 1.6 eV (~ 775 nm)[28], thus the rutile phase has a higher reflectance in the IR region since the incident light at a frequency below the plasma frequency leads to motion in the charge carriers that acts to screen out the incident field, in other words, to reflect the incident waves.[29]

The switching behavior of VO_2 thin film can be more clearly elucidated by means of thermal hysteresis loops. **Figure 4b** shows the loops of VO_2-Ge and VO_2-Grphene-Ge samples

Journal of Materials Chemistry C Accepted Manuscript

measured at wavelengths of 650 nm and 2000 nm. For the two samples, the loop measured at 650 nm exhibits a very small contrast in the reflectance spectra compared with that at 2000 nm. In effect, the switching capability is prominent in the spectral range from the wavelength of 1000 nm to 2500 nm, as seen in **Figure 4a**. One can note that the thermal hysteresis loop in the long wavelength region ($\lambda >$ 1000 nm) follows the anticlockwise direction. In contrast, the thermochromism of the VO_2 film in the region from 500 nm to 800 nm is quite on the contrary. The hysteresis loop at 1000 nm follows the clockwise direction, as seen in **Figure 4b**.

According to the hypothesis proposed by Klimov et al.,[30] the hysteresis phenomena during the phase transition were regarded as the integrated outcome of the elementary loops of the grains. This means that the reason for the difference in the hysteresis loop parameters between VO_2 films and bulk single crystals is the presence of a large number of grains of various sizes in VO_2 films. When the VO_2 film is heated up, the growth of a metallic nucleus in the semiconductor phase is stable if the temperature differs from the phase equilibrium temperature (T_c) by a value of ΔT_+. When the film is cooled down, the stable growth of a semiconducting nucleus in the metallic phase takes place, as before, if there is a temperature difference ΔT_-. Since the distributions of grain size are so wide and therefore the deviations ΔT_+ and ΔT_- from T_c for the VO_2 film amount to several tens of degrees (against one or two degrees for the single crystal), the loop for the film is also much wider than that for the single crystal. Moreover, since the transition temperature for a specific grain in the heating process ($T^* = T_c + \Delta T_+$) is larger than that in the cooling process ($T^{**} = T_c - \Delta T_-$), the integral of transition temperature over all the

Journal of Materials Chemistry C Accepted Manuscript

grains in the film brings about the result that the heating branch of the loop is always on the right side, when compared to the cooling branch. As a consequence, the hysteresis loop will follow the anticlockwise direction if the reflectance in the low-temperature phase is smaller than that in the high-temperature phase. In the same way, the loop will follow the clockwise direction if the reflectance in the monoclinic phase is larger than that in the rutile phase. As a matter of fact, very few researches about such an anomalous switching behavior, also reported in the VO_2/sapphire system in the transmittance spectra,[31] were carried out in depth. It remains to be further investigated what causes or affects the existence of anomalous behavior and whether the eccentric phenomenon has the value of practical applications or not.

The transition temperature (defined as the central temperature of the hysteresis loop) of the sandwich-structure sample is around 330 K which is lower than that of VO_2 films on Ge substrate (337 K), let alone lower than that of bulk VO_2 single crystal (Tc ~ 340 K [32]). The Tc value can be reduced in many approaches. First, a slight deviation from stoichiometry[33], either under- or over-stoichiometry, is known to reduce Tc. However, this factor can be eliminated since the valence state of V has been confirmed by the XPS spectra, as seen in **Figure 3a**. Second, the transition temperature can be modified by imposing pressure or uniaxial/biaxial stress[34, 35] or doping[36]. Applying pressure is not an effective method since the volume change at the SMT is much weaker than the c-axis expansion.[37] However, relatively large stress dependence was reported under uniaxial stress along the c-axis of VO_2 ($\mathrm{d}Tc/\mathrm{d}\sigma \approx 1.2\mathrm{K\ kbar^{-1}}$)[38] and the rate at which the transition temperature is modified by the uniaxial stress can be

Journal of Materials Chemistry C Accepted Manuscript

evaluated by the Clausius–Clapeyron equation.[39] Apparently, pressure or uniaxial stress was not imposed here in this work. Third, the total stress in the film, as a combination of thermal stress (tensile) caused by the difference in thermal expansion coefficients (TEC) between film and substrate and the internal stress (compressive) produced by the ion-bombardment effect during the film growth, causes a reduction in *Tc* value. Nevertheless, the transition temperature for the VO_2 film directly grown on Ge substrate was ~ 337 K. The TEC value of graphene is strongly dependent on temperature but remains negative in the temperature range from 300 K to 400 K with a room-temperature value of ~ -8.0×10^{-6} K^{-1}.[40] However, the TEC values are $2.1\times10^{-5} K^{-1}$ [41] and $6.65\times10^{-6} K^{-1}$ [42] for VO_2 and Ge, respectively. That is to say, the middle-layer graphene shrinks when it is exposed to the heat, while the upper-layer VO_2 thin film and the bottom-layer Ge substrate expand. In Lee's and his co-workers' study, they also found the depressed *Tc* value in graphene-supported VO_2 films on the sapphire substrate, and they attributed this phenomenon to the TEC differences.[43] Although the mismatch of TEC between the film and the substrates cannot be eliminated, the intrinsic particularity of graphene should not be neglected here.

Herein, we try to discuss the potential mechanism of the reduction in T_c by the addition of graphene monolayer. Considering the zero-gap and semimetal features of graphene, when it comes to directly contact with semiconductor Ge, especially to directly grow on semiconductor Ge in situ, it is expected that a Schottky barrier will be formed due to the alignment of Fermi level at the interface between semimetal (graphene) and semiconductor (Ge).[44] **Figure 5a** shows

Journal of Materials Chemistry C Accepted Manuscript

the UV-Vis diffuse reflectance spectra of the Graphene/Ge and Ge substrates. The Kubelka–Munk function is adopted to convert the diffuse reflectance measurement into the equivalent absorption coefficient.[45]

$$\alpha = {(1-R)^2}/{2R}$$

where α is the optical absorption coefficient near the absorption edge for indirect interband transition, R is the reflectance of semiconductor, $R = 10^{-A}$, and A is the optical absorbance.

$$\alpha h\nu = C_1(h\nu - E_g)^2$$

$$h\nu = {1240}/{\lambda}$$

where C_1 is the constant for indirect transition, $h\nu$ is the photon energy, E_g is the indirect bandgap energy (eV), and λ is the wavelength (nm).

Figure 5b indicates the $(\alpha h\nu)^{1/2}$ plotted versus $h\nu$ and the vertical segment of the spectra is extended to intersect the $h\nu$ axis to acquire the E_g value of the measured specimen. The E_g value of Ge specimen is 0.625 eV while the Graphene/Ge substrate characterizes an E_g value of 0.592 eV. As apparent from **Figure 5a-b**, the existence of zero-gap graphene in the Graphene/Ge heterostructure contributes to a red shift of the absorption edge, which thus narrows the bandgap of the Ge specimen. The narrowed bandgap demonstrates the Schottky barrier formation and Fermi level alignment at the interface of the Graphene/Ge heterojunction, which thus modifies the electronic structures and influences the optical properties. **Figure 5c** shows the photoluminescence (PL) spectra of the Ge and Graphene/Ge excited by a broadband pulsed UV xenon lamp source. Upon UV irradiation, that is, when Ge is excited by photons with minimal

Journal of Materials Chemistry C Accepted Manuscript

energy equal to its bandgap, electrons transfer to the conduction band from the valence band. After that, the electrons relax extremely fast and rapidly recombine with holes in the valence band. As a consequence, the narrowed bandgap of Graphene/Ge heterostructure can facilitate charge separation to produce electron/hole (e^-/h^+) pairs and thus enhance the PL intensity upon e^-/h^+ recombination, as shown in **Figure 5c**. On the other hand, if the excited electrons can be transferred to another intended target in time, for example, to the VO_2 film, then this attempt may affect the electronic structures and optical properties of the VO_2 film.[46, 47]

In fact, a semimetal-semiconductor junction will be produced when graphene grows on Ge, accompanied by the Schottky barrier formation and Fermi level alignment at the contact interface.[48] During this process, an electronic charge flowing usually occurs. To figure out the electron flowing direction, the energy band diagrams of the interconnecting materials should be taken into consideration. Some previous data[49-53] and the above calculated values are utilized to draw the band structures, as listed in **Table 1**. The vacuum level (E_0) is used as a reference. The work function Φ of graphene is 4.23 eV, which is greater than that of Ge ($\Phi' = 4.1$ eV), namely, the Fermi level E_F' of Ge higher than that of graphene (E_F). As the couple of materials come into contact, electrons will be driven to flow from conduction band of Ge to graphene until their Fermi levels become aligned. In fact, graphene can act as an excellent electron acceptor owing to its 2D π-conjugation structure,[54] which can further facilitate the electrons flowing from Ge to graphene. The energy band diagrams before and after contact are depicted in **Figure 6a-b**. On the other hand, the work function Φ'' of VO_2 is 5.15 eV, which is

Journal of Materials Chemistry C Accepted Manuscript

greater than that of graphene. Once the couple of materials are brought into contact, electrons will be driven to flow from graphene to VO_2 until their Fermi levels alignment at the contact interface. In reality, graphene can also serve as an excellent electron transporter to achieve efficient charge separation due to its 2D planar structure,[55-58] which can further promote the electrons transferring from graphene to VO_2. Moreover, in single-layer graphene, electrons can behave as massless Dirac fermions. **Figure 6c-d** shows the energy band diagrams before and after contact. Here, the Graphene/Ge support behaves as electron donor and provides electrons for VO_2, which thus can increase the electron density in VO_2 film and modify the electronic structure of VO_2.[59] That is to say, such an increase of electron density in VO_2 film, especially upon light irradiation, will consequentially destabilize the semiconductor phase of thermochromic VO_2 film on the basis of the theory of Zylbersztejn and Mott, in which the SMT of VO_2 is shown to be of Mott-Hubbard transition and driven by the increase of electron density. In other words, once the electron density reaches a critical value, the SMT can be triggered and a metal phase can be generated.[1, 60] For example, the critical electron density is approximately 10^{18} ~ 10^{19} cm^{-3} for the Mott transition of bulk VO_2 with T_c ~ 68 °C.[61] Based on these analyses, the SMT of thermochromic VO_2 film may be triggered at a relatively lower temperature rather than at the temperature of ~ 68 °C, as we observed in this study. It is expected that charge transfer to a thermochromic material manipulated by appropriate materials design can induce its structural phase transition. For example, the excited hot carriers formed by surface plasmon resonance (SPR) may be utilized to inject into a thermochromic material to induce its structural phase

Journal of Materials Chemistry C Accepted Manuscript

transition.[62-64] In fact, a recent study has demonstrated that the hot electrons produced by plasmonic Au nanoparticles deposited on MoS_2 layer can induce a transient reversible first-order phase transition in which the Mo coordination changes from a direct band gap semiconducting trigonal prismatic (2H) structure to a metallic octahedral (1T) structure.[65] In a word, we propose that the plausible mechanism behind the present structural phase transition is electron injection and doping to destabilize thermochromic VO_2 film. We hope this study can provide new insights and pave the way for the development of active optical devices to exploit the fantastic electronic and structural properties of 2D structures and materials.

4. Conclusions

In conclusion, vanadium dioxide (VO_2) thin film has been successfully deposited on transfer-free monolayer graphene support by the magnetron sputtering method. The as-prepared VO_2 film has been demonstrated to consist of pure phase with ~ 20 % infrared reflectance contrast in the IR range. For the VO_2-graphene-Ge junction, the presence of graphene interlayer can effectively reduce the SMT temperature of VO_2 thin film from ~ 340 K to ~ 330 K. On the basis of the Mott-Hubbard phase transition theory, a plausible mechanism is proposed here for the first time from the perspective of electron transfer to elucidate the reduced transition temperature of VO_2 film by ~ 10 K, which believes that the electron transfer can increase the electron density in VO_2 film, destabilize the semiconductor phase of VO_2 film and thus decrease the SMT temperature of thermochromic VO_2 film. This investigation may provide insights for

Journal of Materials Chemistry C Accepted Manuscript

choosing graphene as a matrix for thermochromic VO_2 films and offer potential applications in sensors, optical and electrical switches, and other nanodevices.

Acknowledgements

This study was financially supported by the high-tech project of MOST (2014AA032802) and the National Natural Science Foundation of China (No.: 51032008, 51272273, 51102270 and 51272271).

Notes and references

Electronic Supplementary Information (ESI) available: [details of any supplementary information available should be included here]. See DOI:

1. A. Zylbersztejn and N. F. Mott, *Physical Review B*, 1975, **11**, 4383-4395.
2. M. Liu, H. Y. Hwang, H. Tao, A. C. Strikwerda, K. Fan, G. R. Keiser, A. J. Sternbach, K. G. West, S. Kittiwatanakul, J. Lu, S. A. Wolf, F. G. Omenetto, X. Zhang, K. A. Nelson and R. D. Averitt, *Nature*, 2012, **487**, 345-348.
3. L. Whittaker, C. J. Patridge and S. Banerjee, *The Journal of Physical Chemistry Letters*, 2011, **2**, 745-758.
4. M. Gu, S. A. Wolf and J. Lu, *Advanced Materials Interfaces*, 2014, **1**, n/a-n/a.
5. G. Xu, P. Jin, M. Tazawa and K. Yoshimura, *Solar Energy Materials and Solar Cells*, 2004, **83**, 29-37.
6. P. Jin, S. Nakao and S. Tanemura, *Thin Solid Films*, 1998, **324**, 151-158.

Journal of Materials Chemistry C Accepted Manuscript

7. G. Xu, C. M. Huang, M. Tazawa, P. Jin, D. M. Chen and L. Miao, *Applied Physics Letters*, 2008, **93**, 061911.

8. J. Jeong, N. Aetukuri, T. Graf, T. D. Schladt, M. G. Samant and S. S. Parkin, *Science*, 2013, **339**, 1402-1405.

9. D.-H. Qiu, Q.-Y. Wen, Q.-H. Yang, Z. Chen, Y.-L. Jing and H.-W. Zhang, *Acta Physica Sinica*, 2013, **62**, 217201.

10. S. H. Chen, H. Ma, S. B. Wang, N. Shen, J. Xiao, H. Zhou, X. M. Zhao, Y. Li and X. J. Yi, *Thin Solid Films*, 2006, **497**, 267-269.

11. T.-W. Chiu, R.-T. Hong, K. Tonooka and N. Kikuchi, *Thin Solid Films*, 2013, **529**, 119-122.

12. H. Koo, H. You, K.-E. Ko, O. J. Kwon, S.-H. Chang and C. Park, *Applied Surface Science*, 2013, **277**, 237-241.

13. N. B. Aetukuri, A. X. Gray, M. Drouard, M. Cossale, L. Gao, A. H. Reid, R. Kukreja, H. Ohldag, C. A. Jenkins, E. Arenholz, K. P. Roche, H. A. Durr, M. G. Samant and S. S. P. Parkin, *Nat. Phys.*, 2013, **9**, 661-666.

14. J. Ma, G. Xu and L. Miao, in *Sustainable Development of Urban Environment and Building Material, Pts 1-4*, eds. H. Li, Y. F. Liu, M. Guo, R. Zhang and J. Du, 2012, pp. 1365-1368.

15. H. Miyazaki and I. Yasui, *Applied Surface Science*, 2006, **252**, 8367-8370.

Journal of Materials Chemistry C Accepted Manuscript

16. J. H. Seol, I. Jo, A. L. Moore, L. Lindsay, Z. H. Aitken, M. T. Pettes, X. Li, Z. Yao, R. Huang and D. Broido, *Science*, 2010, **328**, 213-216.

17. R. S. Edwards and K. S. Coleman, *Accounts of Chemical Research*, 2012, **46**, 23-30.

18. J.-H. Lee, E. K. Lee, W.-J. Joo, Y. Jang, B.-S. Kim, J. Y. Lim, S.-H. Choi, S. J. Ahn, J. R. Ahn, M.-H. Park, C.-W. Yang, B. L. Choi, S.-W. Hwang and D. Whang, *Science*, 2014, **344**, 286-289.

19. L. G. Cancado, K. Takai, T. Enoki, M. Endo, Y. A. Kim, H. Mizusaki, A. Jorio, L. N. Coelho, R. Magalhaes-Paniago and M. A. Pimenta, *Applied Physics Letters*, 2006, **88**, 163106.

20. R. S. Weatherup, B. C. Bayer, R. Blume, C. Ducati, C. Baehtz, R. Schlögl and S. Hofmann, *Nano Letters*, 2011, **11**, 4154-4160.

21. G. Xu, C. M. Huang, M. Tazawa, P. Jin and L. H. Chen, *Optics Communications*, 2009, **282**, 896-902.

22. X. Li, W. Cai, J. An, S. Kim, J. Nah, D. Yang, R. Piner, A. Velamakanni, I. Jung, E. Tutuc, S. K. Banerjee, L. Colombo and R. S. Ruoff, *Science*, 2009, **324**, 1312-1314.

23. W. Bao, F. Miao, Z. Chen, H. Zhang, W. Jang, C. Dames and C. N. Lau, *Nature Nanotechnology*, 2009, **4**, 562-566.

24. J. Nickl, C. Schild, A. Baiker, M. Hund and A. Wokaun, *Fresenius Journal of Analytical Chemistry*, 1993, **346**, 79-83.

25. N. Liu, Z. Pan, L. Fu, C. Zhang, B. Dai and Z. Liu, *Nano Research*, 2011, **4**, 996-1004.

Journal of Materials Chemistry C Accepted Manuscript

26. A. Fasolino, J. H. Los and M. I. Katsnelson, *Nature Materials*, 2007, **6**, 858-861.

27. M. Kang, S. W. Kim, J.-W. Ryu and T. Noh, *AIP Advances*, 2012, **2**, 012168.

28. B. Felde, W. Niessner, D. Schalch, A. Scharmann and M. Werling, *Thin Solid Films*, 1997, **305**, 61-65.

29. H. Zhou, X. Cao, M. Jiang, S. Bao and P. Jin, *Laser & Photonics Reviews*, 2014, **8**, 617-625.

30. V. A. Klimov, I. O. Timofeeva, S. D. Khanin, E. B. Shadrin, A. V. Ilinskii and F. Silva-Andrade, *Technical Physics*, 2002, **47**, 1134-1139.

31. G. Xu, C. M. Huang, P. Jin, M. Tazawa and D. M. Chen, *Journal of Applied Physics*, 2008, **104**, 053101.

32. F. Morin, *Physical Review Letters*, 1959, **3**, 34-36.

33. C. H. Griffiths and H. K. Eastwood, *Journal of Applied Physics*, 1974, **45**, 2201-2206.

34. Y. Gu, J. Cao, J. Wu and L.-Q. Chen, *J Appl Phys*, 2010, **108**, 083517.

35. S. Kittiwatanakul, S. A. Wolf and J. Lu, *Applied Physics Letters*, 2014, **105**, 073112.

36. J. Nag and R. F. Haglund, Jr., *J Phys-Condens Mat*, 2008, **20**, 264016.

37. J. Cao, Y. Gu, W. Fan, L. Q. Chen, D. F. Ogletree, K. Chen, N. Tamura, M. Kunz, C. Barrett, J. Seidel and J. Wu, *Nano Letters*, 2010, **10**, 2667-2673.

38. L. A. Ladd and W. Paul, *Solid State Communications*, 1969, **7**, 425-428.

39. J. Cao, E. Ertekin, V. Srinivasan, W. Fan, S. Huang, H. Zheng, J. Yim, D. Khanal, D. Ogletree and J. Grossman, *Nature nanotechnology*, 2009, **4**, 732-737.

Journal of Materials Chemistry C Accepted Manuscript

Journal of Materials Chemistry C Accepted Manuscript

40. D. Yoon, Y.-W. Son and H. Cheong, *Nano letters*, 2011, **11**, 3227-3231.

41. F. C. Case, *Journal of Vacuum Science & Technology A*, 1984, **2**, 1509-1512.

42. M. Straumanis and E. Aka, *Journal of Applied Physics*, 2004, **23**, 330-334.

43. H. Kim, Y. Kim, T. Kim, A.-R. Jang, H. Y. Jeong, S. H. Han, D. H. Yoon, H. S. Shin, D. J. Bae and K. S. Kim, *Nanoscale*, 2013, **5**, 2632-2636.

44. S. M. Sze and K. K. Ng, *Physics of Semiconductor Devices*, John Wiley & Sons, 2006.

45. J. Ng, S. Xu, X. Zhang, H. Y. Yang and D. D. Sun, *Advanced Functional Materials*, 2010, **20**, 4287-4294.

46. W. He, H.-K. Kim, W. G. Wamer, D. Melka, J. H. Callahan and J.-J. Yin, *Journal of the American Chemical Society*, 2013, **136**, 750-757.

47. W. He, H. Wu, W. G. Wamer, H.-K. Kim, J. Zheng, H. Jia, Z. Zheng and J.-J. Yin, *ACS Applied Materials & Interfaces*, 2014, **6**, 15527-15535.

48. H. Yang, J. Heo, S. Park, H. J. Song, D. H. Seo, K.-E. Byun, P. Kim, I. Yoo, H.-J. Chung and K. Kim, *Science*, 2012, **336**, 1140-1143.

49. C. Ko, Z. Yang and S. Ramanathan, *ACS Applied Materials & Interfaces*, 2011, **3**, 3396-3401.

50. S. Biermann, A. Poteryaev, A. I. Lichtenstein and A. Georges, *Physical Review Letters*, 2005, **94**, 4.

51. V. Eyert, *Annalen Der Physik*, 2002, **11**, 650-702.

52. H. E. Romero, N. Shen, P. Joshi, H. R. Gutierrez, S. A. Tadigadapa, J. O. Sofo and P. C. Eklund, *ACS Nano*, 2008, **2**, 2037-2044.

53. A. Dimoulas, P. Tsipas, A. Sotiropoulos and E. K. Evangelou, *Applied Physics Letters*, 2006, **89**, 252110.

54. Q. Liu, Z. Liu, X. Zhang, L. Yang, N. Zhang, G. Pan, S. Yin, Y. Chen and J. Wei, *Advanced Functional Materials*, 2009, **19**, 894-904.

55. K. S. Novoselov, A. K. Geim, S. V. Morozov, D. Jiang, Y. Zhang, S. V. Dubonos, I. V. Grigorieva and A. A. Firsov, *Science*, 2004, **306**, 666-669.

56. N. Yang, J. Zhai, D. Wang, Y. Chen and L. Jiang, *Acs Nano*, 2010, **4**, 887-894.

57. J. S. Lee, K. H. You and C. B. Park, *Advanced Materials*, 2012, **24**, 1084-1088.

58. X. Pan, G. Ren, M. N. F. Hoque, S. Bayne, K. Zhu and Z. Fan, *Advanced Materials Interfaces*, 2014, **1**, n/a-n/a.

59. H. Lüth, *Solid Surfaces, Interfaces and Thin Films*, Springer, Berlin, 2010.

60. M. S. Laad, L. Craco and E. Mueller-Hartmann, *Physical Review B*, 2006, **73**.

61. P. P. Boriskov, A. A. Velichko, A. L. Pergament, G. B. Stefanovich and D. G. Stefanovich, *Technical Physics Letters*, 2002, **28**, 406-408.

62. M. L. Brongersma, N. J. Halas and P. Nordlander, *Nat Nano*, 2015, **10**, 25-34.

63. A. N. Grigorenko, M. Polini and K. S. Novoselov, *Nat Photon*, 2012, **6**, 749-758.

64. J. Li, H. Zhou, S. Qian, Z. Liu, J. Feng, P. Jin and X. Liu, *Applied Physics Letters*, 2014, **104**, 261110.

Journal of Materials Chemistry C Accepted Manuscript

65. Y. Kang, S. Najmaei, Z. Liu, Y. Bao, Y. Wang, X. Zhu, N. J. Halas, P. Nordlander, P. M. Ajayan, J. Lou and Z. Fang, *Adv. Mater.*, 2014, **26**, 6467-6471.

Journal of Materials Chemistry C Accepted Manuscript

Table 1. Data for the energy level positions of VO_2, graphene and Ge.

Materials	Φ (eV)	E_g (eV)	χ (eV)	E_c (eV)	E_v (eV)
VO_2 (M1)	5.15[49]	0.6[50, 51]	4.85^{α}	-4.85^{α}	-5.45^{α}
Graphene	4.23[52]				
Ge	4.1^{α}	0.625^{α}	4[53]	-4^{α}	-4.625^{α}

Notes: E_0, vacuum level; E_F, Fermi level; Φ, work function; E_g, bandgap; χ, electron affinity; E_c, conduction band; E_v, valence band; α, Calculated values.

Journal of Materials Chemistry C Accepted Manuscript

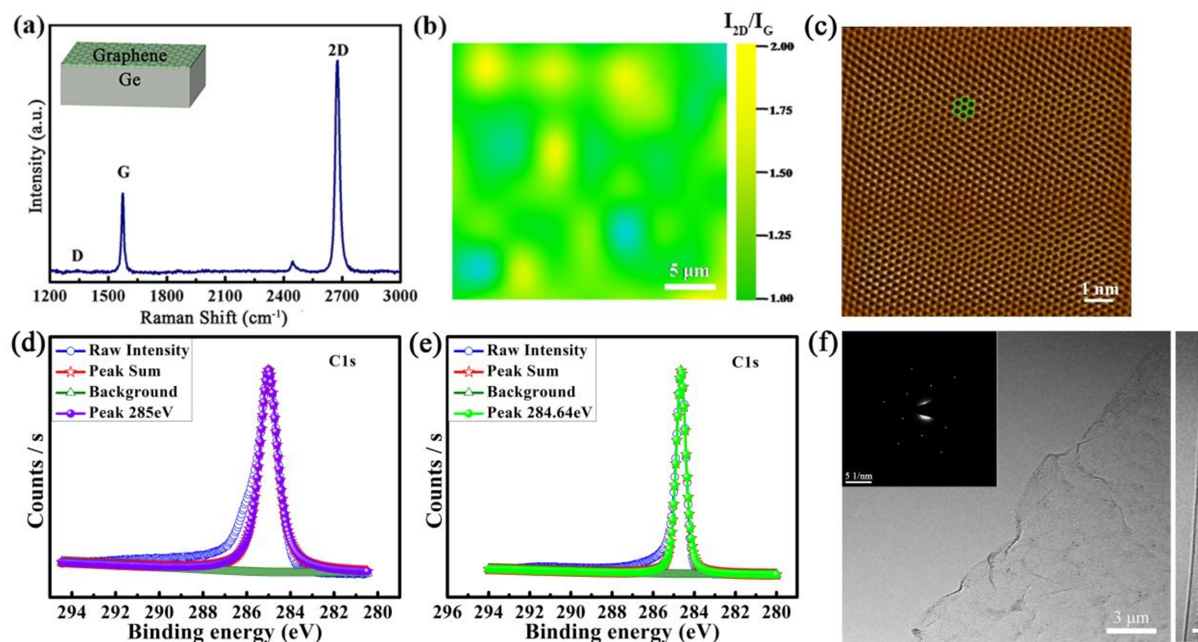

Figure 1. (**a**) Raman spectrum of the graphene directly grown on Ge, inserted with the schematic illustration for Graphene/Ge substrate. (**b**) Two-dimensional Raman mapping of the I_{2D}/I_G peak intensity ratios obtained from the graphene deposited on Ge (a randomly selected 25 μm × 25 μm region with the spot size of 1 μm and the step size of 1 μm). (**c**) STM topography image of the graphene layer on Ge. (**d-e**) XPS analysis results showing the C 1s XPS spectra acquired from the surfaces of Ge (**d**) and Graphene/Ge (**e**). (**f**) TEM image of the transferred graphene film from Ge, inserted with the corresponding SAED pattern. The right inset in (**f**) shows the corresponding HR-TEM image of monolayer graphene edge with one carbon layer, with a scale bar of 3 nm.

Journal of Materials Chemistry C Accepted Manuscript

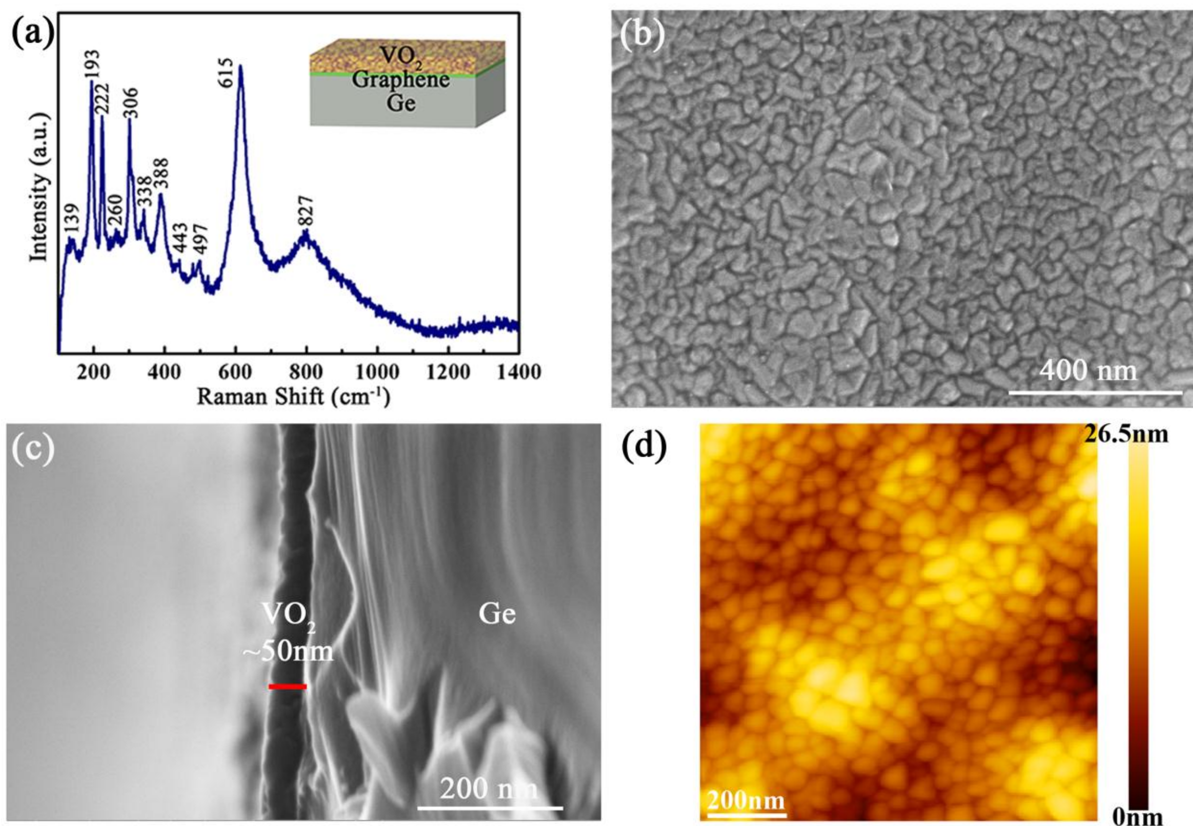

Figure 2. (**a**) Raman spectrum of the VO_2 thin film deposited on Graphene/Ge support, inserted with the schematic illustration for the VO_2-graphene-Ge junction. (**b**) Surface morphology of the VO_2 thin film on Graphene/Ge support examined by SEM. (**c**) Cross-sectional view of the VO_2-graphene-Ge junction examined by SEM. (**d**) Surface topography of the VO_2 thin film grown on Graphene/Ge support examined by AFM.

Journal of Materials Chemistry C Accepted Manuscript

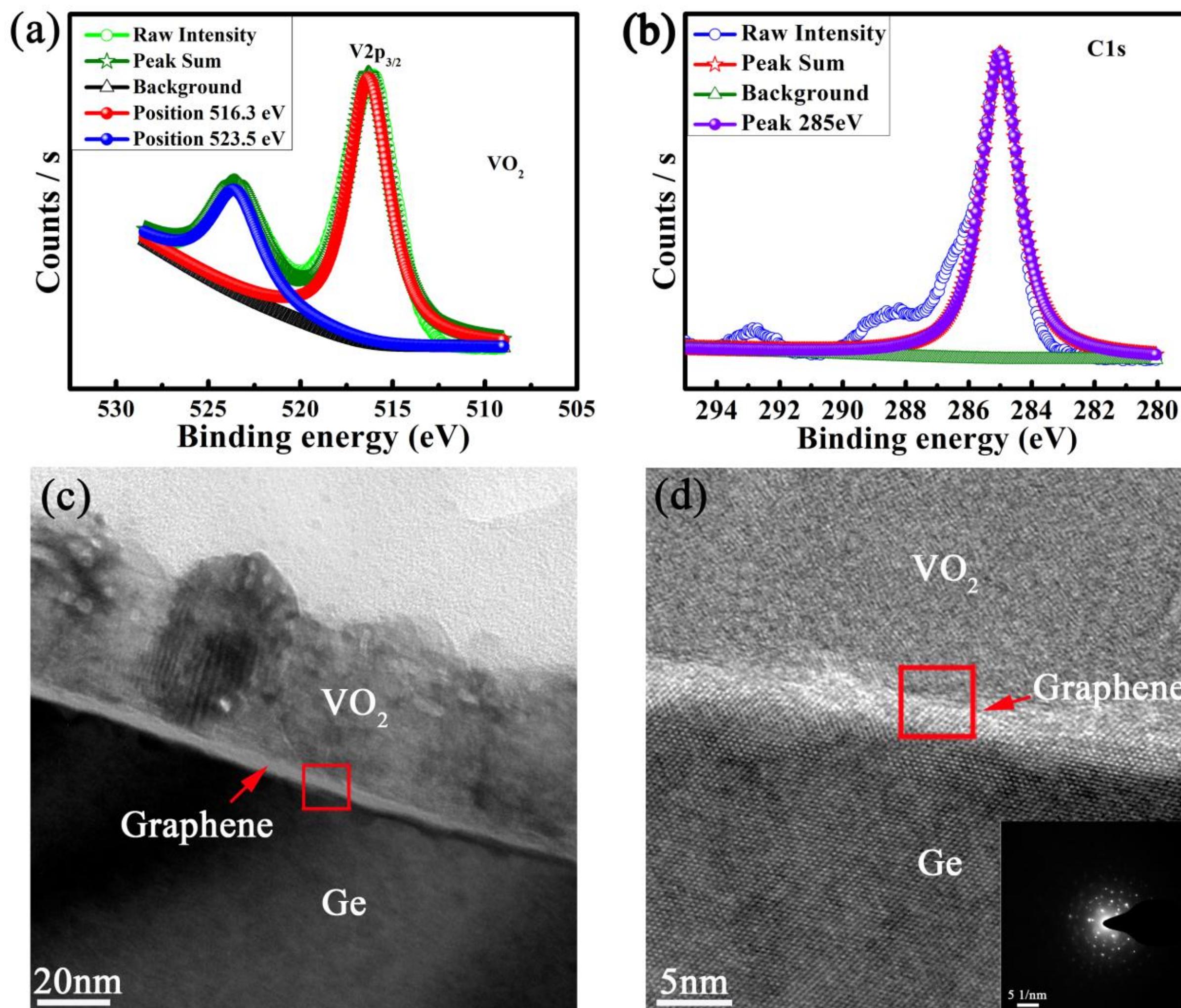

Figure 3. (**a**) XPS analysis result showing the V 2p XPS spectrum obtained from the surface of VO_2 thin film grown on Graphene/Ge support. (**b**) XPS analysis result showing the C 1s XPS spectrum acquired from the surface of VO_2 thin film on Graphene/Ge support. (**c**) Cross-sectional view of the VO_2-graphene-Ge junction examined by TEM, showing the top-layer VO_2, middle-layer graphene and bottom-layer Ge. (**d**) HR-TEM image of the VO_2-graphene-Ge junction corresponding to the red rectangular area in (**c**). The inset in (**d**) shows the SAED pattern corresponding to the red rectangular area in (**d**).

Journal of Materials Chemistry C Accepted Manuscript

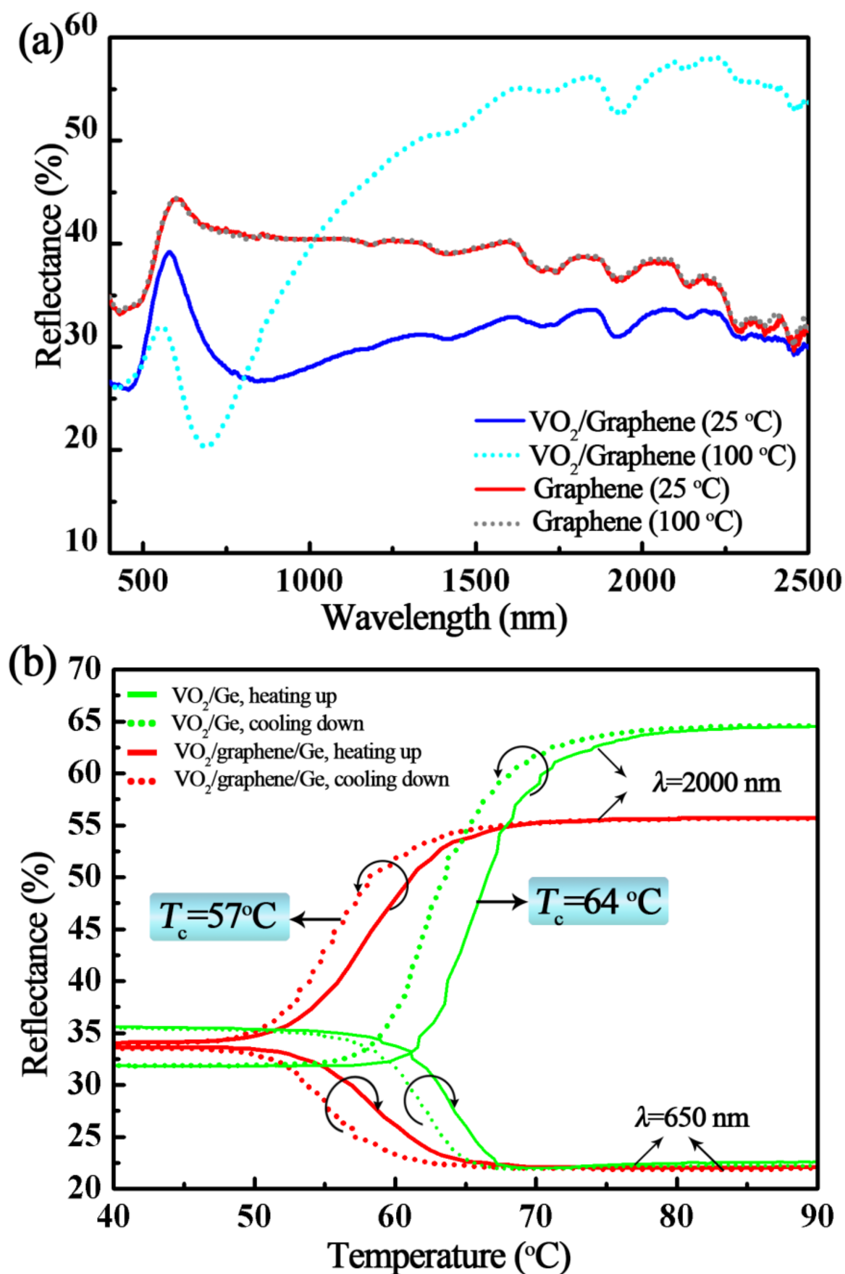

Figure 4. (**a**) Reflectance spectra of the Graphene/Ge and the VO_2 thin film grown on the Graphene/Ge support. **(b)** Thermal hysteresis loops of reflectance measured at the wavelengths of 650 nm and 2000 nm for the VO_2 thin film on Ge and Graphene/Ge support.

Journal of Materials Chemistry C Accepted Manuscript

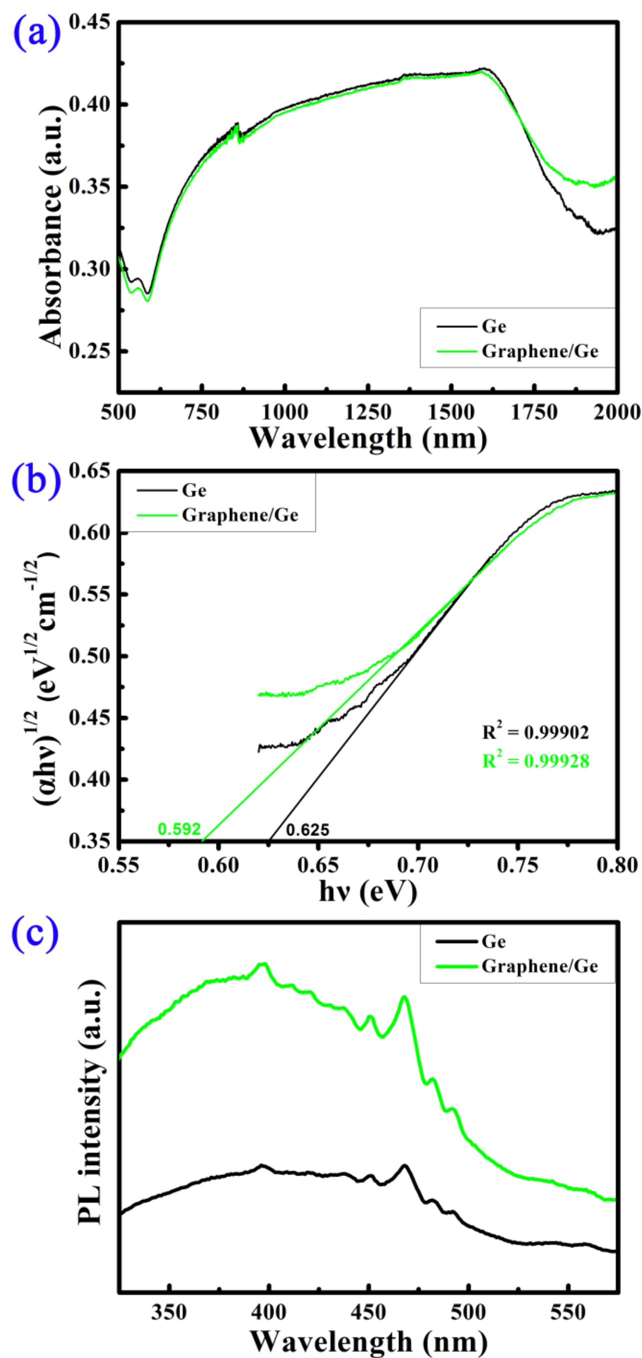

Figure 5. (**a**) UV-Vis-NIR diffuse reflectance spectra of the Ge and Graphene/Ge, accompanied by the corresponding Kubelka–Munk transformed reflectance spectra (**b**). (**c**) Photoluminescence (PL) spectra obtained from the surfaces of Ge and Graphene/Ge.

Journal of Materials Chemistry C Accepted Manuscript

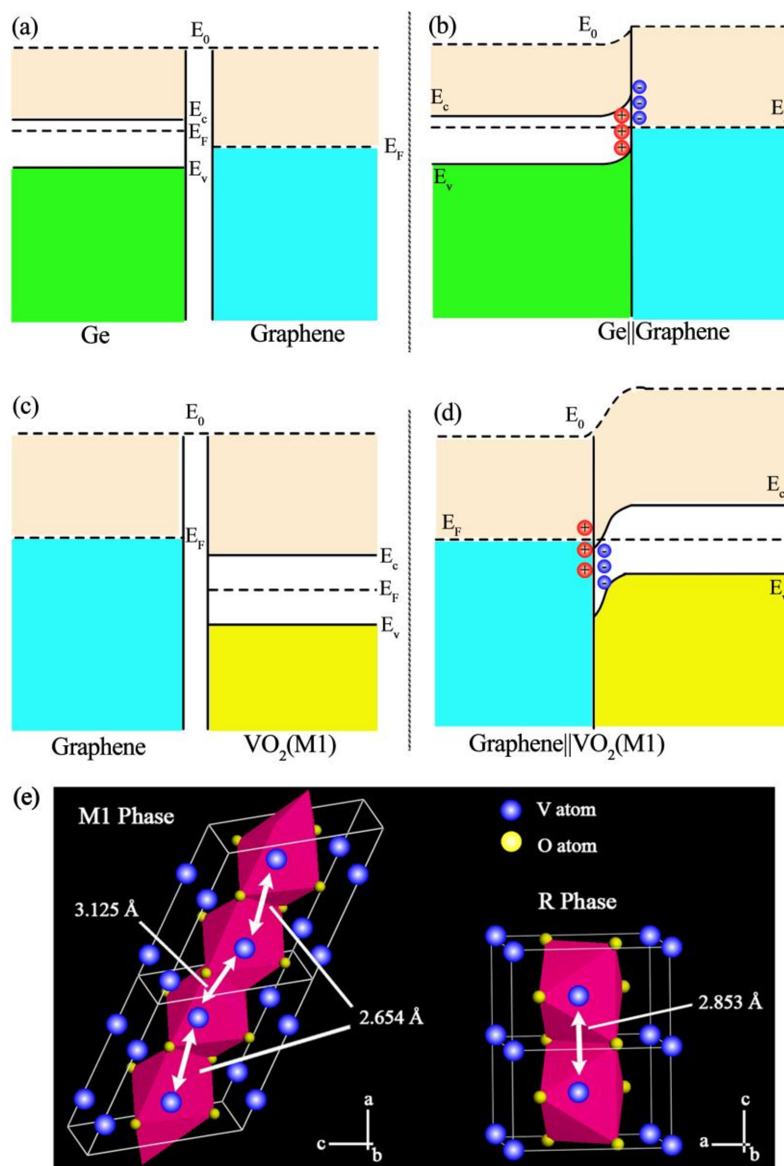

Figure 6. (**a-b**) Energy band diagrams of graphene and Ge before (**a**) and after (**b**) contact. (**c-d**) Energy band diagrams of graphene and VO_2 before (**c**) and after (**d**) contact. (**e**) The crystallographic structure of VO_2 (M1) and VO_2 (R). Upon semiconductor-to-metal transition (SMT), the linear equidistant V-V chains along *c*-axis (2.853 Å) in tetragonal R phase will become distorted with alternative spacings of 3.125 Å and 2.654 Å in monoclinic M phase.

Journal of Materials Chemistry C Accepted Manuscript

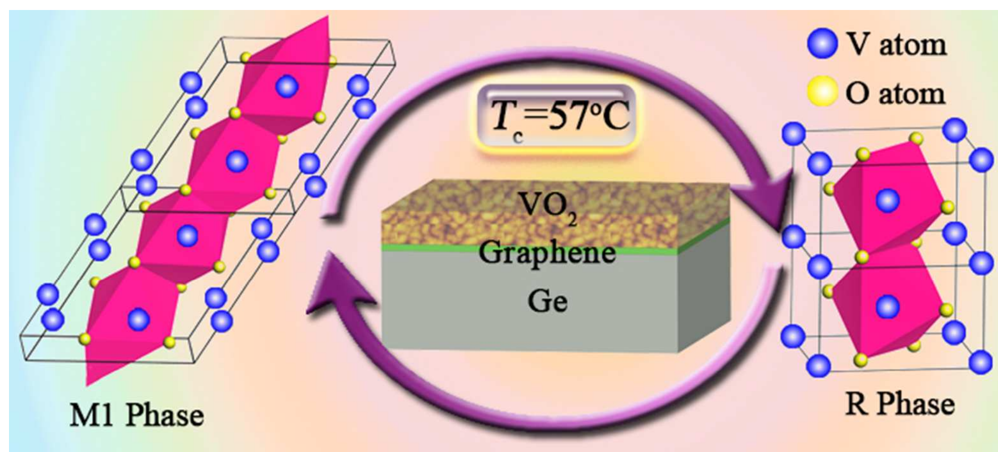

Graphical abstract
250x112mm (72 x 72 DPI)

Journal of Materials Chemistry C Accepted Manuscript